



Contents lists available at ScienceDirect

Chemical Engineering Science

journal homepage: www.elsevier.com/locate/ces

Measurement of dynamic capillary pressure and viscosity via the multi-sample micro-slit rheometer

Doyoung Moon, Kalman B. Migler*

Polymers Division, 100 Bureau Drive, NIST, Gaithersburg, Maryland 20899, USA

ARTICLE INFO

Article history:

Received 14 October 2008

Received in revised form 30 January 2009

Accepted 18 February 2009

Keywords:

Imbibition

Dynamic capillary pressure

Contact angle

Microfluidics

Viscosity

Rheometer

ABSTRACT

We develop two direct methods to simultaneously measure the dynamic capillary pressure and the viscosity of fluids by application of differential forces during flow into micro-channels. In the first method, a series of external pressures is applied in conjunction with the dynamic capillary pressure and a “Bagley analysis” is applied to the flow front velocity, and in the second, we utilize differential gravitational forces. By explicitly measuring the dynamic capillary pressure, the measurement window of the recently developed multi-sample micro-slit rheometer is extended to the regime where capillary forces are significant. These measurement methods will be useful in understanding filling flows encountered in diverse areas such as microfluidics, oil recovery and biological transport.

Published by Elsevier Ltd.

1. Introduction

¹The flow of fluids into micro and nanoscale pores is critically important in many applications such as viscometry (Srivastava et al., 2005; Srivastava and Burns, 2006), microfluidics (Squires and Quake, 2005), oil recovery (Hatiboglu and Babadagli, 2008), ink printing (Ridgway and Gane, 2002), tribology, dip-pen nanolithography (Tas et al., 2002) and transport in plants and living organisms (Schneider et al., 2000). The dynamics of the filling process is governed by a balance of pressures: capillary, viscous, gravitational and external. While viscous and gravitational pressures are readily measured, the dynamic capillary pressure is difficult to measure because it is coupled with the fluid’s contact angle with the wall and with flow induced changes in the fluid structure, both of which vary with shear rate (Degennes, 1985). In this manuscript, we demonstrate a simple method based on the “Bagley analysis” for extraction of the dynamic capillary pressure from an analysis of the velocity of the fluid flow front.

In a capillary driven flow of fluid into a pore, the capillary number (ratio of viscous to capillary forces—see Table 1) at the fluid-air-wall interface plays a critical role. In previous studies (Hoffman, 1975), the dynamic capillary pressure, P_{cap} , has been calculated by starting with the quiescent capillary pressure and adding a correction term that is induced by the dynamic contact angle

$$P_{cap} = 2\gamma \cos(\theta) \left(\frac{1}{h} + \frac{1}{w} \right) \quad (1)$$

* Corresponding author.

E-mail address: Kalman.Migler@nist.gov (K.B. Migler).

¹ Official contribution of the National Institute of Standards and Technology; not subject to copyright in the United States.

(for the case of a rectangular capillary) where γ is the surface tension, θ is the contact angle, and h and w are rectangular channel depth and width, respectively. But in practice, θ and γ may not be possible to measure— θ is difficult to measure in non-circular or micro-geometries geometries (Ichikawa et al., 2004; Kim and Whitesides, 1997) and is generally shear rate dependent while γ may differ from its quiescent value if the fluid is multi-component (Nath, 1999).

There are several numerical and experimental results for filling flow analysis in micro-channels, but they wrestle with the issue of the dynamic contact angle and dynamic capillary pressure (Kim et al., 2002; Choi et al., 2006). Capillary pressure can be obtained by direct measurement (Weitz et al., 1987; Calvo et al., 1991; Degennes, 1988), but the methodologies have several limitations such as applicability only to liquid/liquid systems, requiring flow through porous media or requiring independent viscosity data. Alternatively, the dynamic contact angle (Hoffman, 1975; Fermigier and Jenffer, 1991) measurement can be obtained and then the dynamic capillary pressure are estimated indirectly with Eq. (1), but the method only applies to dimensions of mm’s order that are accessible by simple optical techniques. This has the limitations described previously.

Our immediate need for an accurate and robust measurement of the dynamic capillary pressure stems from our development of an instrument to measure fluid rheology at low volumes. The recently developed multi-sample micro-slit rheometer (MMR) is a pressure driven slit rheometer with miniaturized dimensions (Moon et al., 2008). The principle of operation is to apply an external gas pressure to the reservoir of the fluid/polymer of interest and track the velocity of the flow front as it fills the micro-channel. As the fluid fills the channel, it slows down due to the increasing flow resistance. By relating the flow front velocity to the fluid shear rate, we measure the viscosity as a function of shear rate. The device has been

Table 1

Dimensionless numbers for micro-channel flow and their meaning where h is the characteristic length (the slit channel height in our system), flow velocity V_f , viscosity η , density ρ , surface tension of the fluid γ .

Dimensionless number	Notation	Formula	Meaning
Capillary number	Ca	$Ca = \frac{\eta V_f}{\gamma}$	Viscous Force Capillary Force
Bond number	Bo	$Bo = \frac{\rho g h^2}{\gamma}$	Gravity Force Capillary Force
Reynolds number	Re	$Re = \frac{\rho V_f h}{\eta}$	Inertia Force Viscous Force
Weber number	We	$We = \frac{\rho V_f^2 h}{\gamma}$	Inertia Force Capillary Force

demonstrated with volumes of 30 μL over a range of temperatures on polymer melts and solutions ranging in viscosity from 1 to 10^6 Pa s. In the previous demonstrations of the instrument, the applied minimum shear stress is much greater than that of theoretical maximum capillary force so the capillary pressure is safely ignored. However, in order to measure the rheological properties of fluids in the case of low capillary number (in practice, for viscosity less than 1 Pa s), the dynamic capillary pressure must be independently determined.

In this work we develop two methods to simultaneously determine P_{cap} , both based on the application of differential pressure. In the first case, we show that we can utilize a modified Bagley analysis (Bagley, 1957) to obtain the dynamic capillary pressure based on application of differential external pressure at the same shear rate. In the second, use the combined effect of capillary and gravity forces without an external pressure source. Once we determine P_{cap} , the viscosity calculation is straightforward.

2. Differential forces methods

For a steady flow of a Newtonian fluid in a unidirectional slit channel of length l , and height h , the viscosity η , can be measured by Agassant et al. (1991)

$$\eta = \frac{\tau_w}{\dot{\gamma}_a} = \frac{h}{2} \left(\frac{\Delta P}{l} \right) \frac{1}{6 V_f} = \frac{h^2 \Delta P}{12 l V_f} \quad (2)$$

where τ_w and $\dot{\gamma}_a$ are wall shear stress and apparent shear rate respectively, ΔP is the pressure drop along the channel and V_f is the average flow velocity. We assume the ratio of width w to depth, h , is sufficiently large enough that the side wall effect can be ignored and that inertial effects are negligible (Carreau et al., 1997). In a filling flow, where the fluid displaces air as it enters the channel, Eq. (2) can still be used provided that

$$\Delta P = P_{ext} + P_{cap} + P_{grav} \quad (3)$$

and that l is identified with the length of the fluid in the channel, rather than the total channel length.

2.1. Case I: differential external pressure

In the first method to measure the dynamic capillary pressure and viscosity, we utilize the Bagley analysis which was originally developed to separate out the pressure drop in capillary rheology of polymeric materials that stems from the extensional flow fields in the entry and exit regions from that which stems from the Poiseuille flow in the capillary itself. This is necessary in polymers because the extensional viscosity can differ greatly from the simple shear viscosity resulting in significant deviations between apparent viscosity and actual viscosity. The fundamental idea is to carry out a series of experiments where the shear rate is kept constant but the channel length varies. In the data analysis, plots of the total pressure drop at constant shear rate as a function of length are extrapolated to

the pressure drop at zero length. This extrapolated pressure drop at zero flow length is due to the entrance and exit flow. In the previous MMR experiments on high viscosity melts and solutions, modification of the classic Bagley method was necessary because the MMR utilizes a filling flow rather than the more common flow through a filled capillary tube. The extrapolated pressure drop was identified with the sum of the entrance flow plus the drop due to velocity rearrangements at the flow front.

In the present case of low viscosity Newtonian fluids where the fluid can spontaneously flow into the micro-channel, we recognize that we can identify the pressure drop that occurs at the flow front with the dynamic capillary pressure. This is possible because the pressure drop in the entrance is negligible because the fluids have low elasticity and that experiments are conducted under conditions of large l/h . In our system, the range of the Reynolds number Re is 10^{-4} –1 for shear rate; $(1-10^3)\text{s}^{-1}$, fluid density; 10^3 kg/m^3 , channel depth; 10^{-4} m, fluid viscosities; $(10^{-2}-10^{-1})\text{Pa s}$. With these parameters, the maximum loss of fluid kinetic energy (inertia effect, $1/2 \rho V_f^2$) is below 10 Pa in the entrance region which falls within the experimental uncertainty. Furthermore, once the capillary pressure as a function of shear rate is obtained, we can calculate the viscosity and deduce the dynamic contact angle as a function of shear rate.

2.2. Case II: differential gravitational pressure

For the second method to determine capillary pressure and viscosity, instead of varying the external pressure as in the above section, we add a gravitational pressure to either enhance or retard the capillary driven flow. The viscosity for a slit channel can be expressed as follows by adding gravitational force to the total pressure drop term of Eq. (2),

$$\text{Upward flow : } \eta_{up} = \frac{\tau_w}{\dot{\gamma}_a} = \frac{h^2 (P_{cap}^{up} - \rho g l_{up})}{12 l_{up} V_{up}} \quad (4a)$$

$$\text{Downward flow : } \eta_{dw} = \frac{\tau_w}{\dot{\gamma}_a} = \frac{h^2 (P_{cap}^{dw} + \rho g l_{dw})}{12 l_{dw} V_{dw}} \quad (4b)$$

where ρ is density of fluid, g is the gravitational acceleration constant, l_{dw} , l_{up} are the flow lengths in the downward and upward directions, respectively, $\rho g l$ is the hydraulic pressure due to gravitational force, V_{dw} , V_{up} are flow velocity, and P_{cap}^{dw} , P_{cap}^{up} are the dynamic capillary pressures. Several conditions must be met for these equations to be valid: the dynamic capillary number is sufficiently low ($Ca < 1$), the gravitational force is comparable with dynamic capillary force (Bond number, $Bo \approx 1$), and the inertial force is sufficiently small compared with capillary and viscous force (Weber number, $We \ll 1$, Reynolds number, $Re < 1$). The requirement that Bo is sufficiently large so that gravitational effects measurably perturb the flow has the practical constraint that only data at relatively large l is meaningful. This leads to a limited shear range over which we can make the measurements. Here, over the limited shear rate range, we introduce the assumption that the capillary pressure and the viscosity in the upward and downward flows are equal, and we then equate Eqs. (4a) and (4b) to yield

$$P_{cap} = \frac{\rho g (l_{up} + k l_{dw})}{(1 - k)} \quad (5)$$

where $k = l_{up} V_{up} / l_{dw} V_{dw}$. Eq. (5) indicates that the capillary pressure can be obtained by a measurement of flow velocity as a function of length.

Finally, the viscosity can be determined by applying P_{cap} to the horizontal flow equation (Eq. (2)). This relation can be applied to a shear thinning fluid if the capillary pressure is evaluated at the same flow velocity for the two opposite vertical channels and can

be applied at the location where the horizontal flow velocity has the same shear rate (Fig. 1).

3. Experimental procedure

The device for this experiment was originally designed as a pressure driven (slit) rheometer under conditions of relatively high

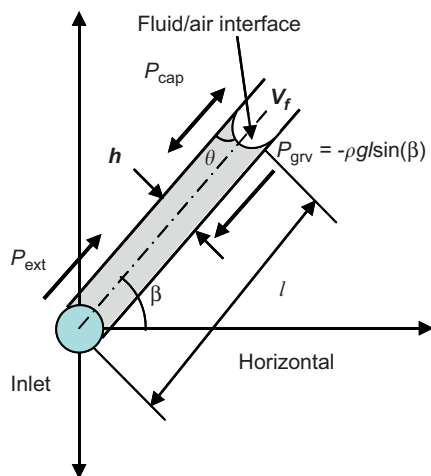


Fig. 1. Three pressures acting in a tilted micro-channel. P_{ext} is externally imposed, P_{cap} is due to capillary forces at the flow front and P_{grv} is due to gravity force (ρ and g is a fluid density and gravitational constant, respectively, β is a tilting angle, l is a flow length), h is the channel height (132 μm in our system), V_f is a flow velocity. Case 1: $\beta = 0$, flow from P_{ext} and P_{cap} ; Case 2: $\beta \neq 0$ and $P_{ext} = 0$, flow from P_{cap} and P_{grv} .

pressure ($> 10 \text{ kPa}$). For the current lower pressure experiments ($< 10 \text{ kPa}$) with lower viscosity fluids ($< 1 \text{ Pa s}$), we modified the sample loading chamber as described in Fig. 2, for the differential pressure experiments, and Fig. 3, for the differential gravitational experiments, in order to prevent uncontrolled capillary driven flow during the sample loading process. In Fig. 2, the sample loading assembly consists of two concentric tubes so that the sample fluid is loaded through the inner tube from a syringe, while the outer tube independently provides the pressurized gas. A computer controlled

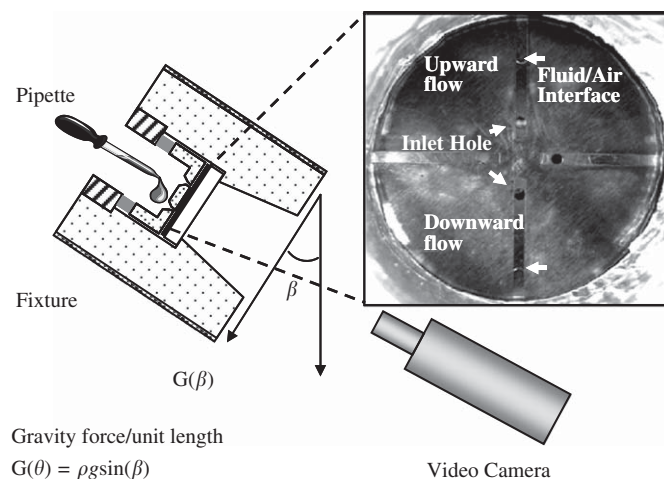


Fig. 3. Experimental setup for Case II experiments where the differential pressures are due to gravity, which retards or enhances the flow.

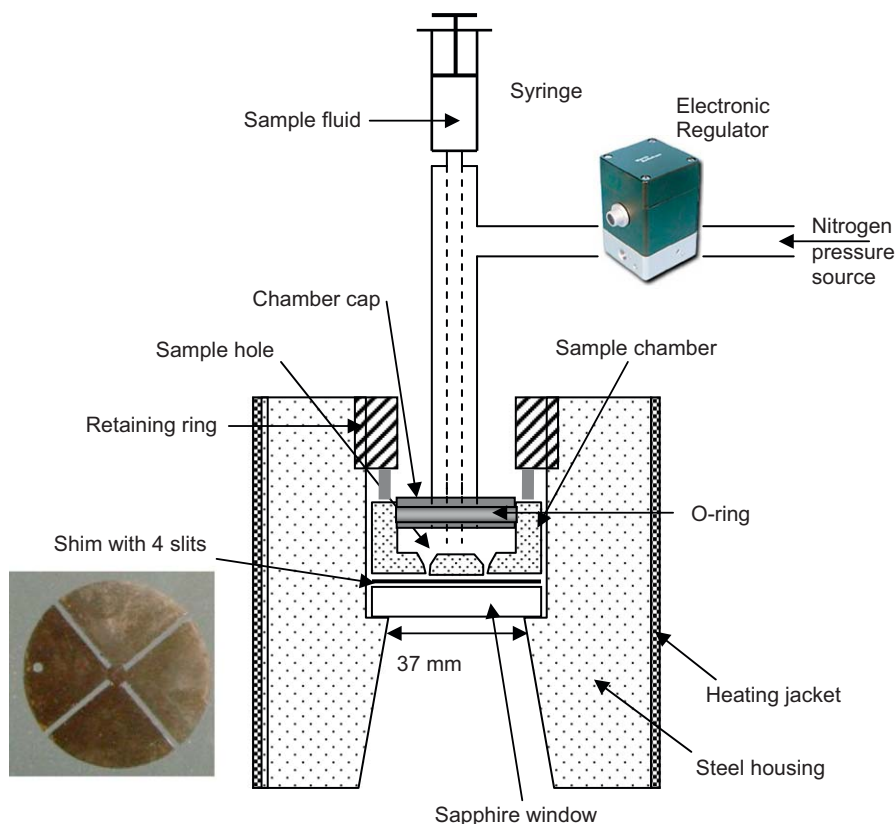


Fig. 2. Fixture diagram of the experiment for Case I experiments where flow is driven by external pressure in conjunction with dynamic capillary pressure. There are 4 slit channels at right angles to each other (slit depth 132 μm , maximum viewing channel length 13 mm).

Table 2
Properties of standard viscosity materials for the experiment.

Materials	Viscosity (mPa s)	Density (Kg/L)	Surface tension at 22 °C (mN/m) ^a	Formulation ^b
Std. Oil #1 20 °C (N250) 50 °C	648.3 129.6	842.1 824.1	29.7 ± 0.060	Poly-alpha-olefin
Std. Oil #2 20 °C (N44) 50 °C	92.11 24.34	828.0 809.4	28.7 ± 0.016	Poly-alpha-olefin
Std. Oil #3 20 °C (S6) 50 °C	9.558 3.808	877.8 857.6	29.2 ± 0.042	Mineral oil

^aPendent drop method.

^bFrom material safety data sheet of CANNON Instrument Company.

electronic pressure regulator (Model: T3210 1 PSI, Bellofram²) with a maximum pressure of 6900 Pa (1 psi) and control resolution of 69 Pa (0.01 psi) was utilized and the pressure was confirmed through a U-tube manometer. Briefly, there are four slit channels in the MMR which are formed using a thin (132 μm thickness, 1.3 mm width, 13 mm effective length) metal shim sandwiched between a stainless steel sample chamber and a sapphire window (47 mm diameter, 5 mm thickness). The flow front is recorded via video camera and its velocity as a function of time and length is obtained utilizing video analysis software. Additional details are described in our previous paper (Moon et al., 2008).

For the differential gravitational experiments, the fixture is tilted by an angle β , so that the flow in one channel contains an upward component, a second channel contains a downward component and two channels remain horizontal. Samples were manually loaded into the sample chambers through disposable glass pipettes. For elevated temperatures ($\approx 50^\circ\text{C}$) the samples were heated in a water bath and then rapidly loaded into the heated instrument. As the sample chamber has a depth of 3 mm, there is an associated gravitation hydraulic pressure that must be considered in the analysis.

Three viscosity standard Newtonian fluids (CANNON Instrument Company, USA) were used for the reference fluids and their certified data were compared to the results of the experiments. The properties of the standard fluids are expressed in Table 2. The standard fluids are selected so that the viscosities are roughly 10 (for fluid S6), 100 (for fluid N44), 1000 (for fluid N250) times higher than that of water at room temperature. The surface tension at the air/fluid interface was measured by the pendent drop method (I.T. Concept, Longessaigne, France). With these flow channel dimensions, external pressures and fluid viscosities, we meet the above criteria laid out for the dimensionless parameters in the shear rate range used in the present experiments (1–1000) s⁻¹.

4. Results and discussion

Fig. 4 plots the apparent viscosity ($\eta_a = h^2 P_{ext} / 12 V_f l$) as a function of shear rate for the Case I experiments consisting of application of a series of external pressures (P_{ext}). η_a ignores the contribution from P_{cap} and thus is useful for examining discrepancies with the true viscosity, η . Fig. 4 shows that the deviation of η_a from the true viscosity (Ref. data) becomes greater as either P_{ext} decreases and/or the shear rate decreases. For $P_{ext} > 1$ kPa, the apparent viscosity and true viscosity begin to converge.

Quantitatively, the dynamic capillary pressure can be extracted from the experiment plotted in Fig. 4 via the Bagley analysis. For a given curve of Fig. 4, taken at a fixed pressure, each datum corre-

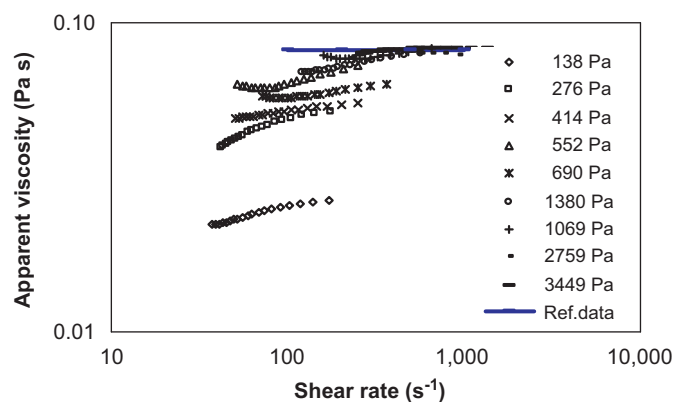


Fig. 4. Apparent viscosity (which ignores P_{cap}) versus shear rate for a series of external pressures, P_{ext} for the Case I experiment. The apparent viscosity approaches the true viscosity as P_{ext} approaches 1 kPa.

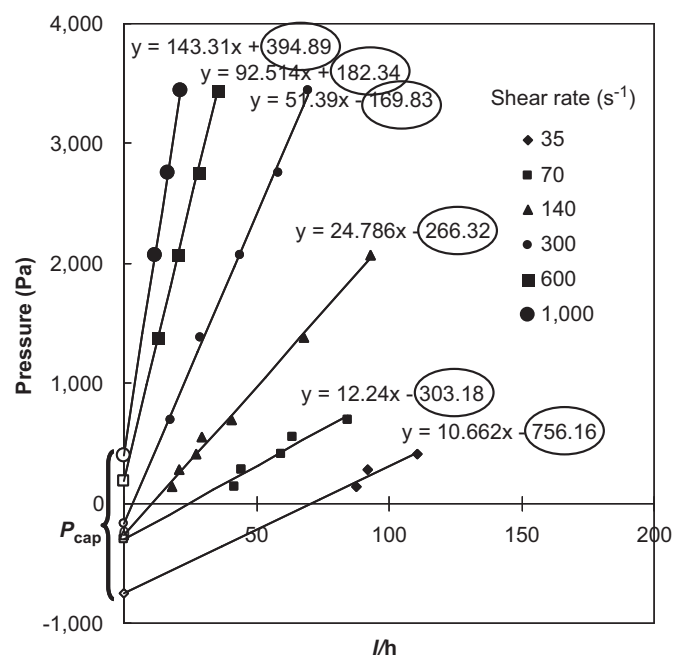


Fig. 5. Bagley plot to obtain the dynamic capillary pressure. The open symbols are the dynamic capillary pressure, P_{cap} , at each shear rate, determined by extrapolating the flow curves to zero length ($l/h = 0$).

² Certain equipment, instruments or materials are identified in this paper in order to adequately specify the experimental details. Such identification does not imply recommendation by the National Institute of Standards and Technology nor does it imply the materials are necessarily the best available for the purpose.

sponds to a different length l —higher shear rates corresponding to shorter l . Fig. 5 then shows a plot of P_{ext} versus l/h for a series of shear rates from 35 to 1000 s⁻¹. Note that the iso-bar experiments

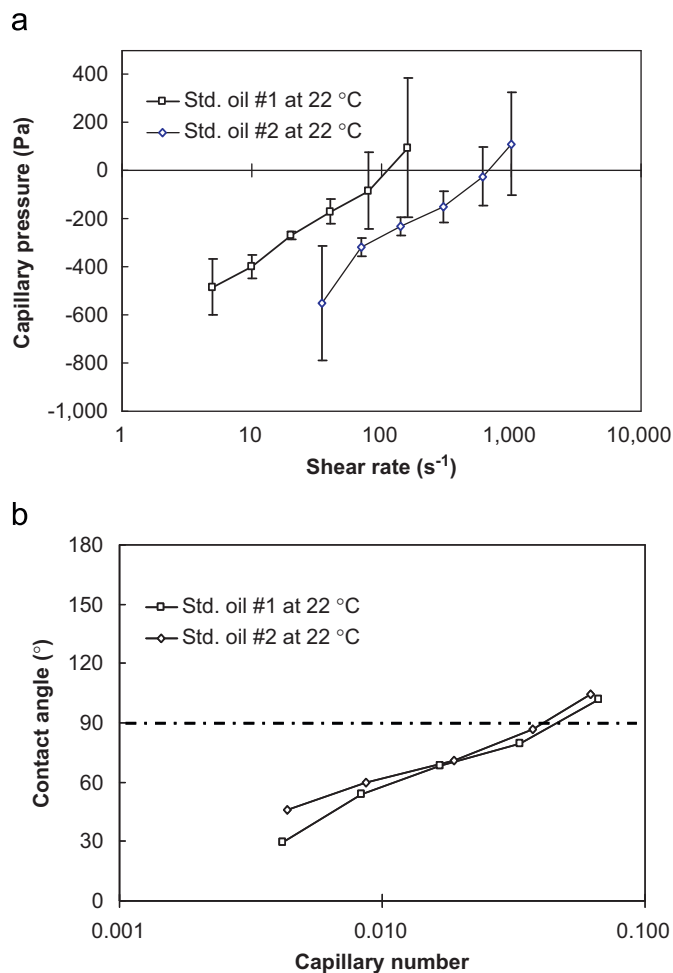


Fig. 6. Dynamic capillary pressure versus shear rate and the corresponding contact angle versus capillary number.

(as shown in the lines in Fig. 4) now show up in Fig. 5 as a series of horizontal data points where each successive data point corresponds to a different shear rate, as indicated in the legend. The six lines in Fig. 5 connect the different experimental runs at different pressures for which the shear rates coincide. Extrapolation of these curves to $l/h = 0$ yields P_{cap} for each shear rate. The shear rate dependence of the capillary pressure is shown in Fig. 6a. Through the dynamic capillary pressure from Fig. 6a along with the channel dimensions and surface tension (Table 2), we can calculate the dynamic contact angle by solving Eq. (1) for θ , as shown in Fig. 6b. These results agree closely with a direct measurement of the dynamic contact angle (Hoffman, 1975).

The underlying assumption of this analysis procedure is that the linear extrapolation of the curves of P_{ext} versus l/h is to $l/h = 0$ does in fact yield P_{cap} . The linearity of the curves over which there is high quality data, such as for $\dot{\gamma} = 300 \text{ s}^{-1}$ gives confidence to this extrapolation process. Fluids of greater complexity than the simple oils tested here may possess a time dependence to their response, and this may manifest in a non-linear curve.

The data in Fig. 6 yields a simple physical picture, at high shear rates, the contact angle is above $\pi/2$ and thus the dynamic capillary pressure is negative. As the fluid slows down in the capillary, the contact angle decreases causing an increase in the capillary pressure which acts to pull the fluid into the channel. The experimental uncertainty was obtained by repeating the five experimental sets of

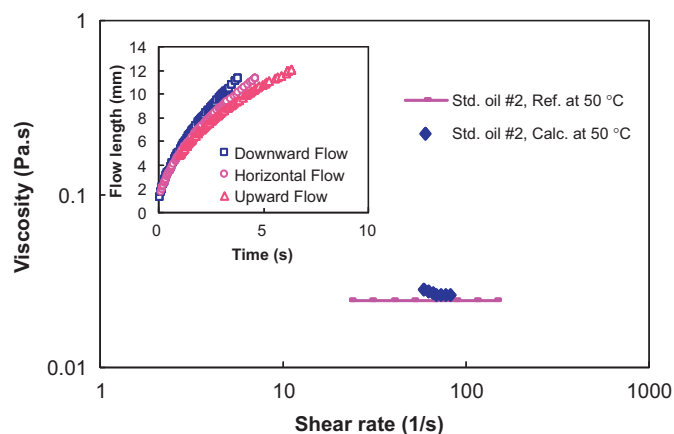


Fig. 7. Estimated viscosity by the gravity/capillary force (Case II) method. The viscosity was evaluated only in the region where the ratio of gravity/capillary pressure was larger than 0.15. Inset graph shows the raw data for the flow length versus time for three channels aligned differently with respect to gravity.

nine pressure experiments and is relatively high at the lowest and highest shear rates. Once the capillary pressure is known, the true viscosity can be easily calculated as a function of shear rate using Eqs. (2) and (3).

In the second method, we utilize the gravitational differences to extract the viscosity and the dynamic capillary pressure, as described previously. A typical result of flow length versus time is represented in an inset graph of Fig. 7 for three channels: upwards (the slowest), downward (the fastest) and horizontal. Once the data of flow length versus time is obtained, the capillary pressure and viscosity are determined. We only utilized data where that the ratio of the gravity to capillary force exceeds 15% so that Eqs. (4a), (4b) and (5) contain experimentally meaningful differences between the upward and downward flows. The obtained viscosity agrees well with the certified reference values as shown in Fig. 7. The range of values of the capillary pressure is expressed in Fig. 8 for three different fluids at two different temperatures. The values of the dynamic capillary pressure in this method range from -500 to -250 Pa, which overlap within experimental uncertainty with those from the Bagley analysis. The results from the Cases I and II methods are summarized in Fig. 9. For Case I, two standard oils (#1, #2) show good agreement with reference data. For standard oil #3, the capillary pressure could not be measured with the current apparatus due to limitations in standard video frame rate and the limited channel length. The uncertainty of the viscosity data is depends on the uncertainty of P_{cap} from Fig. 6a. The filled symbols in Fig. 9 show the viscosity for the Case II experiments.

5. Conclusions

We summarize the viscosity results from the two methods in Fig. 9. The advantages of the differential pressure (Bagley) method is that it can capture a broader range of shear rates—in principle the shear rate range can be brought much lower by application of a negative pressure. The Bagley method then provides a straightforward way to extract the dynamic capillary pressure. An advantage of the differential gravitational method is the inherent simplicity (no external pressure source) and its ability to capture lower shear rates. These methods are generally applicable to shear thinning fluids.

In previous work, we demonstrated that the MMR successfully measured the viscosity of polymer melts in the viscosity range of $1-10^6$ Pa.s. In this work, we extended the MMR to lower viscosity

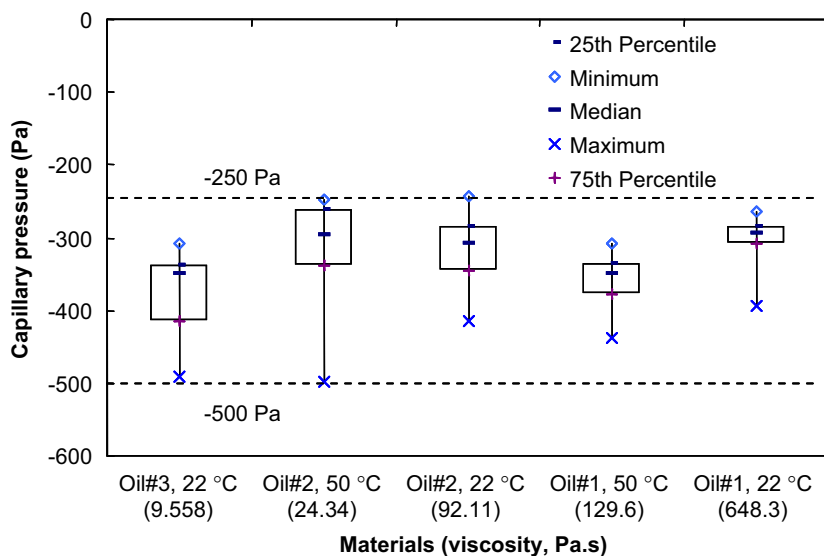


Fig. 8. Dynamic capillary pressure obtained from Case II experiment for three different fluids.

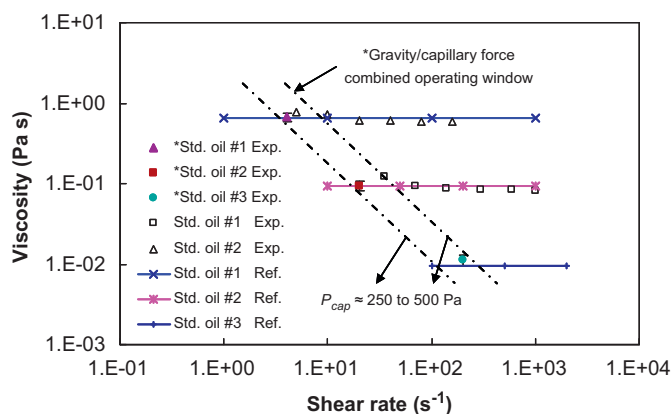


Fig. 9. Comparison of the results obtained from Case I (open symbols) and Case II (closed symbols). The experimental results show good agreement between the two methods and with the reference values of three standard viscosity materials.

fluids (down to 0.01 Pa s) by developing methods to measure the dynamic capillary pressure. These methods for measurement of viscosity and dynamic capillary pressure should find a broad range of applications, from micro-fluidics to oil-recovery.

References

- Agassant, J.-F., Avenas, P., Sergent, J.-P.H., Carreau, P.J., 1991. *Polymer Processing: Principles and Modeling*. Carl Hanser Verlag.
- Bagley, E.B., 1957. End corrections in the capillary flow of polyethylene. *Journal of Applied Physics* 28, 624–627.
- Carreau, P.J., De Kee, D., Chhabra, R.P., 1997. *Rheology of Polymeric Systems: Principles and Applications*. Munich, Hanser Publishers, Hanser/Gardner Publications, New York, Cincinnati.
- Calvo, A., Paterson, I., Chertcoff, R., Rosen, M., Hulin, J.P., 1991. Dynamic capillary-pressure variations in diphasic flows through glass-capillaries. *Journal of Colloid and Interface Science* 141, 384–394.

- Choi, D.S., Lee, S.W., Lee, S.S., Im, Y.T., 2006. Micro-channel flow analysis by a fringe element reconstruction method. *Journal of Micromechanics and Microengineering* 16, 571–579.
- Degennes, P.G., 1985. Wetting-statics and dynamics. *Reviews of Modern Physics* 57, 827–863.
- Degennes, P.G., 1988. Dynamic capillary-pressure in porous-media. *Europhysics Letters* 5, 689–691.
- Fermigier, M., Jenffer, P., 1991. An experimental investigation of the dynamic contact-angle in liquid liquid-systems. *Journal of Colloid and Interface Science* 146, 226–241.
- Hatiboglu, C.U., Babadagli, T., 2008. Pore-scale studies of spontaneous imbibition into oil-saturated porous media. *Physical Review E* 77.
- Hoffman, R.L., 1975. Study of advancing interface.1. Interface shape in liquid-gas systems. *Journal of Colloid and Interface Science* 50, 228–241.
- Ichikawa, N., Hosokawa, K., Maeda, R., 2004. Interface motion of capillary-driven flow in rectangular microchannel. *Journal of Colloid and Interface Science* 280, 155–164.
- Kim, E., Whitesides, G.M., 1997. Imbibition and flow of wetting liquids in noncircular capillaries. *Journal of Physical Chemistry B* 101, 855–863.
- Kim, D.S., Lee, K.C., Kwon, T.H., Lee, S.S., 2002. Micro-channel filling flow considering surface tension effect. *Journal of Micromechanics and Microengineering* 12, 236–246.
- Moon, D., Bur, A.J., Migler, K.B., 2008. Multi-sample micro-slit rheometry. *Journal of Rheology* 52, 1131–1142.
- Nath, S., 1999. Surface tension of nonideal binary liquid mixtures as a function of composition. *Journal of Colloid and Interface Science* 209, 116–122.
- Ridgway, C.J., Gane, P.A.C., 2002. Controlling the absorption dynamic of water-based ink into porous pigmented coating structures to enhance print performance. *Nordic Pulp & Paper Research Journal* 17, 119–129.
- Schneider, H., Wistuba, N., Wagner, H.J., Thurmer, F., Zimmermann, U., 2000. Water rise kinetics in refilling xylem after desiccation in a resurrection plant. *New Phytologist* 148, 221–238.
- Srivastava, N., Davenport, R.D., Burns, M.A., 2005. Nanoliter viscometer for analyzing blood plasma and other liquid samples. *Analytical Chemistry* 77, 383–392.
- Srivastava, N., Burns, M.A., 2006. Analysis of non-Newtonian liquids using a microfluidic capillary viscometer. *Analytical Chemistry* 78, 1690–1696.
- Squires, T.M., Quake, S.R., 2005. Microfluidics: fluid physics at the nanoliter scale. *Reviews of Modern Physics* 77, 977–1026.
- Tas, N.R., Berenschot, J.W., Mela, P., Jansen, H.V., Elwenspoek, M., van den Berg, A., 2002. 2D-confined nanochannels fabricated by conventional micromachining. *Nano Letters* 2, 1031–1032.
- Weitz, D.A., Stokes, J.P., Ball, R.C., Kushnick, A.P., 1987. Dynamic capillary-pressure in porous-media-origin of the viscous-fingering length scale. *Physical Review Letters* 59, 2967–2970.